

Supplementary Information

Ultrabright fluorescent silica nanoparticles for in vivo targeting xenografted human tumors and cancer cells in zebrafish

Saquib Ahmed M. A. Peerzade^a, Xiaodan Qi^{b#}, Fabrice J.F. Laroche^{b#}, Shajesh Palantavida^{c,††}, Maxim Dokukin^{c,†††}, Berney Peng^{a,d}, Hui Feng^{b*}, Igor Sokolov^{a,c,e*}

^a. Department of Biomedical Engineering, Tufts University, Medford, MA 02155, USA. Email: igor.sokolov@tufts.edu

^b. Departments of Pharmacology and Medicine, The Cancer Research Center, Section of Hematology and Medical Oncology, Boston University School of Medicine, Boston, MA, USA. Email: huifeng@bu.edu

^c. Department of Mechanical Engineering, Tufts University, Medford, MA 02155, USA.

^d. NanoScience Solutions, LLC, 200 Boston Ave 2103, Medford, MA 02155, USA.

^e. Department of Physics, Tufts University, Medford, MA 02155, USA.

†† Present address: Center for Nano and Material Sciences, Jain University, Jakkasandra, Kanakapura, Karnataka 562112 India.

††† National Research Nuclear University MEPhI, Moscow, 115409 Russia

Equal contribution

equal contribution

* corresponding authors

Contents

1. Absorbance measurement used to identify the range of excitation wavelengths for the excitation and emission matrix.....	2
2. Atomic force microscopy	2
3. Measurements for quantifying amount of folic acid molecules per PF127 molecule.....	4
4. Measurements for quantifying the amount of folic acid molecules per particle.....	6
5. Measurements for quantifying brightness and quantum yield of the particles	8
6. Tagging ability of UFMS particles using human cervical epithelial cancer (HeLa) cells in vitro.....	12
7. Control experiments: Tagging ability of UFMS particles HeLa and Hs578t cells in vitro...	14
8. Tagging ability of UFMS particles using xenographic HeLa tumors in zebrafish in vivo ...	15
10. Schematics of the synthesis	17
11. Zebrafish Image Processing: sensitivity calculation in zebrafish model.....	18
12. Cell toxicity study	21
13. Additional control experiments in vivo	23
SUPPLEMENTARY REFERENCES.....	25

1. Absorbance measurement used to identify the range of excitation wavelengths for the excitation and emission matrix

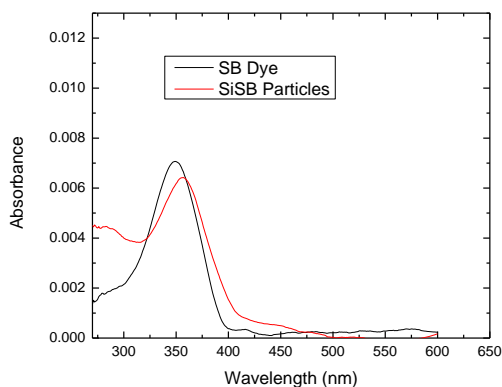


Figure S1: Absorbance of SiSB particles (red) and SB dye (black) used to measure the excitation-emission matrix.

Absorbance spectra of dyes and particles (figure S1) used to measure the excitation and emission spectra as shown in figure 1A and 1B respectively. Figure S1 shows the absorbance spectra of SB dye and SiSB particles, which was measured to decide which wavelengths a self-excitation to use for the excitation and emission matrix of Sb dye and SiSB particles is shown in figure 1A and 1B. Absorbance maximum of dye/particles is 350nm is seen in figure S1.

2. Atomic force microscopy

Figure S2A shows an AFM image of well dispersed mesoporous silica nanoparticles. Figure S2C and S2D show number and intensity size distribution measured using DLS respectively. From Table S1 and S2, it can be seen that the size of the particles measured using AFM is $\sim 29 \pm 5$ nm while that measured using DLS (number weighted mean) is 35 ± 2 nm. From the AFM image (S2A) and PDI of 0.14, it can be said that the particles are well dispersed and not agglomerated.

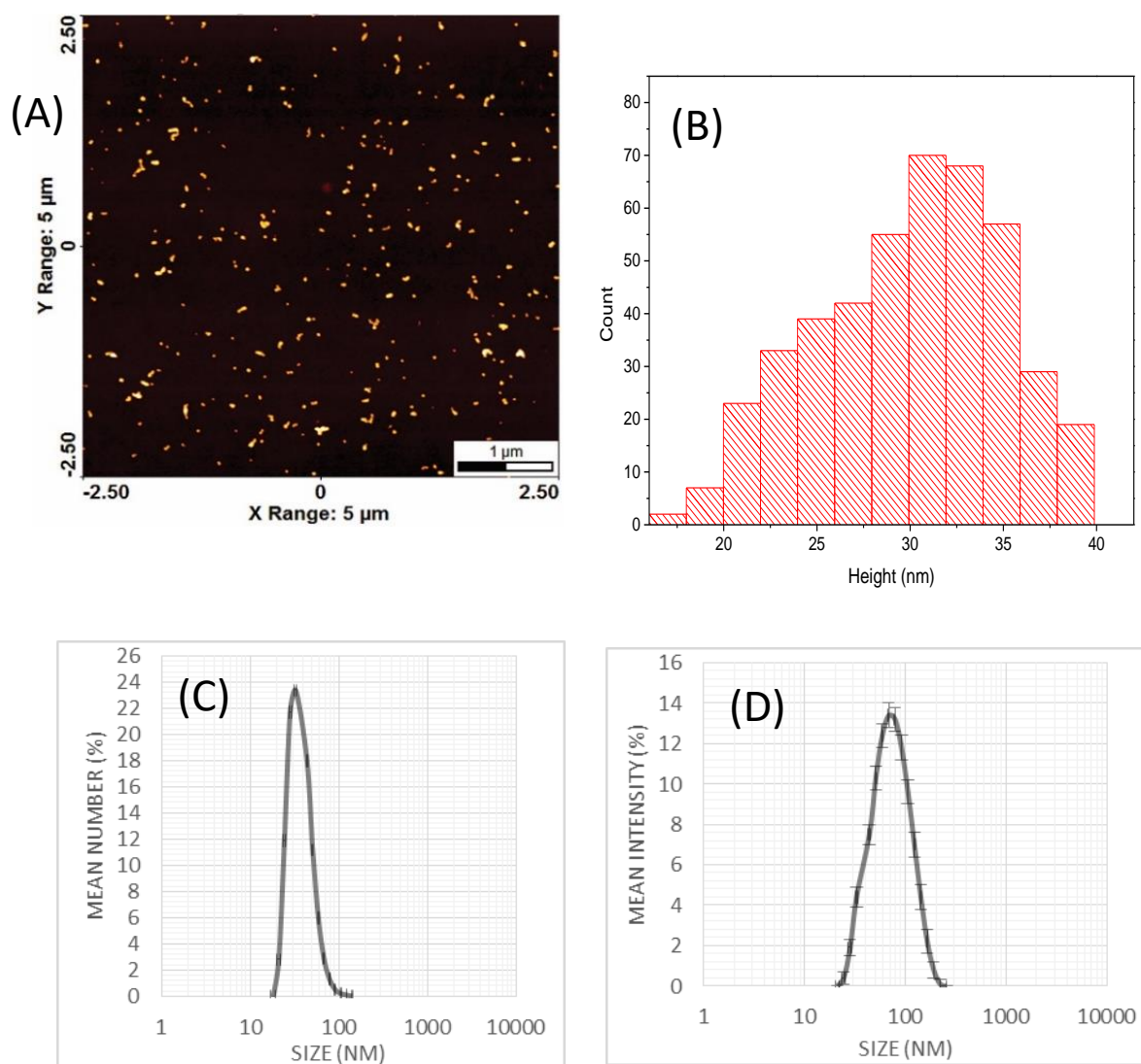


Figure S2: Size distribution of mesoporous silica nanoparticles measured using AFM. (A) AFM image processed through particle recognition software (SPIP), (B) Mean number and (C) mean intensity and (D) size distribution measured using DLS.

Table S1: Mean, minimum, median and maximum calculated using AFM based size distribution of mesoporous silica nanoparticles (figure S2).

N total	Mean	Sum	Minimum	Median	Maximum
444.00	29 ± 5 nm	13286.46	17.01 nm	30.49 nm	39.59 nm

Table S2: Number mean, Intensity mean, Zaverage and Polydispersity index (PDI) of mesoporous silica nanoparticles measured using DLS.

Number Mean	Intensity Mean	Zaverage	PDI
35 ± 2 nm	70 ± 1 nm	60 ± 1 nm	0.14

3. Measurements for quantifying amount of folic acid molecules per PF127 molecule

To calculate the efficiency of PF127-folic acid synthesis the number of folic acid per PF127 molecule was estimated. Absorbance (figure S3) and known extinction coefficient ¹⁻⁴ was used to calculate the concentration of folic acid (in moles/liter). The concentration of PF127 in moles/liter was calculated using concentration in mg/mL and molecular weight. The number of folic acid per PF127 molecules is the ratio of concentrations of FA to PF127. Assuming a maximum number of 2 folic acid groups is attached per PF127 molecule (Table S3) the efficiency of folic acid attachment is ~60%.

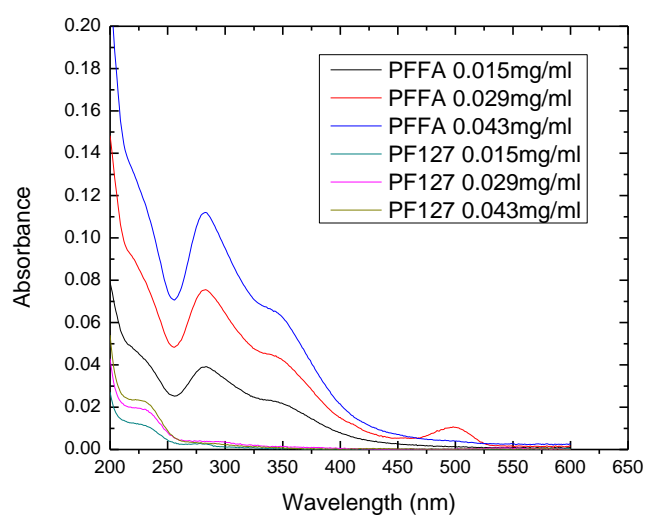


Figure S3: Absorbance of PF127-folic acid (PFFA) with increase in concentration 0.015 (blue), 0.03 (green) and 0.045 (red) mg/mL and of control PF127 with increase in concentration 0.015 (cyan), 0.03 (purple) and 0.045 (yellow) mg/mL.

Table S3: Calculating the number of folic acid molecules per PF127 molecule using absorbance and extinction coefficient¹⁻⁴.

Concentration mg/mL	Wavelength nm	Extinction Coefficient $M^{-1}cm^{-1}$	# of FA molecules per PF127 molecule
0.015	344	7150	2.8 ± 0.1
0.029	344	7150	2.8 ± 0.1
0.043	344	7150	2.8 ± 0.1
0.015	363	6197	2.6 ± 0.1
0.029	363	6197	2.5 ± 0.1
0.043	363	6197	2.6 ± 0.1
0.015	282	27000	1.22 ± 0.05

0.029	282	27000	1.22 ± 0.05
0.043	282	27000	1.25 ± 0.05

4. Measurements for quantifying the amount of folic acid molecules per particle

The number of folic acid groups was calculated using the absorbance and extinction coefficient at 282 nm ($27000 \text{ M}^{-1}\text{cm}^{-1}$). Because of the known concentration of the particles, we can estimate the total amount of folic acid groups per particle. In the case of the use of amine-folic acid conjugate, some of the folates can be encapsulated inside the volume of the particles. Therefore, these density numbers should be treated as an upper limit for those particles.

When the calculation of the number of folates is based on the absorbance, it is important to remove the contribution non-folate part of the particle, see Figure S4. To do that, the absorbance of SiSB-PEG at $\sim 350 \text{ nm}$ was normalized to that of the folic acid-conjugated nanoparticles (Figure S4 A-D). Then, the absorbance due to folic acid will be equal to the difference between the absorbances of folate- functionalized particles and the same particles without folate at 282 nm. The results of these estimations are shown in Table S2.

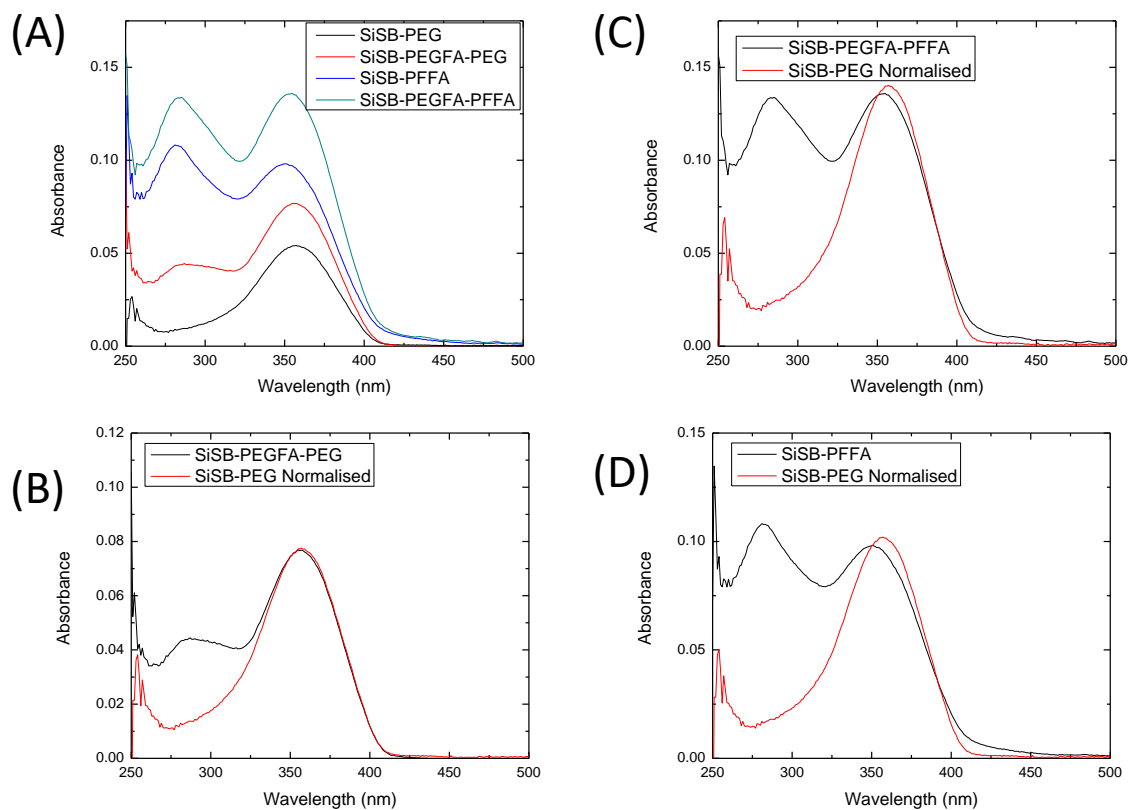


Figure S4: Absorbance spectra (A) of SiSB-PEG (black), SiSB-PEGFA (red), SiSB-PFFA (blue) and SiSB-PEGFA-PFFA (green) particles. Normalized absorbance spectra of SiSB-PEG to the maximum absorbance peak at 350 nm of SiSB-PEGFA (B), SiSB-PEGFA-PFFA (C) and SiSB-PFFA (D) particles.

Table S4: Number of folic acid groups per nm^2 of SiSB-PGEGFA-PEG, SiSB-PFFA and SiSB-PEGFA-PFFA nanoparticles estimated using the absorbance and extinction coefficient of folic acid.

Particle Type	# of FA molecules per nm^2
SiSB-PEGFA-PEG	0.21 ± 0.02
SiSB-PFFA	0.78 ± 0.05
SiSB-PEGFA-PFFA	0.90 ± 0.09

5. Measurements for quantifying brightness and quantum yield of the particles

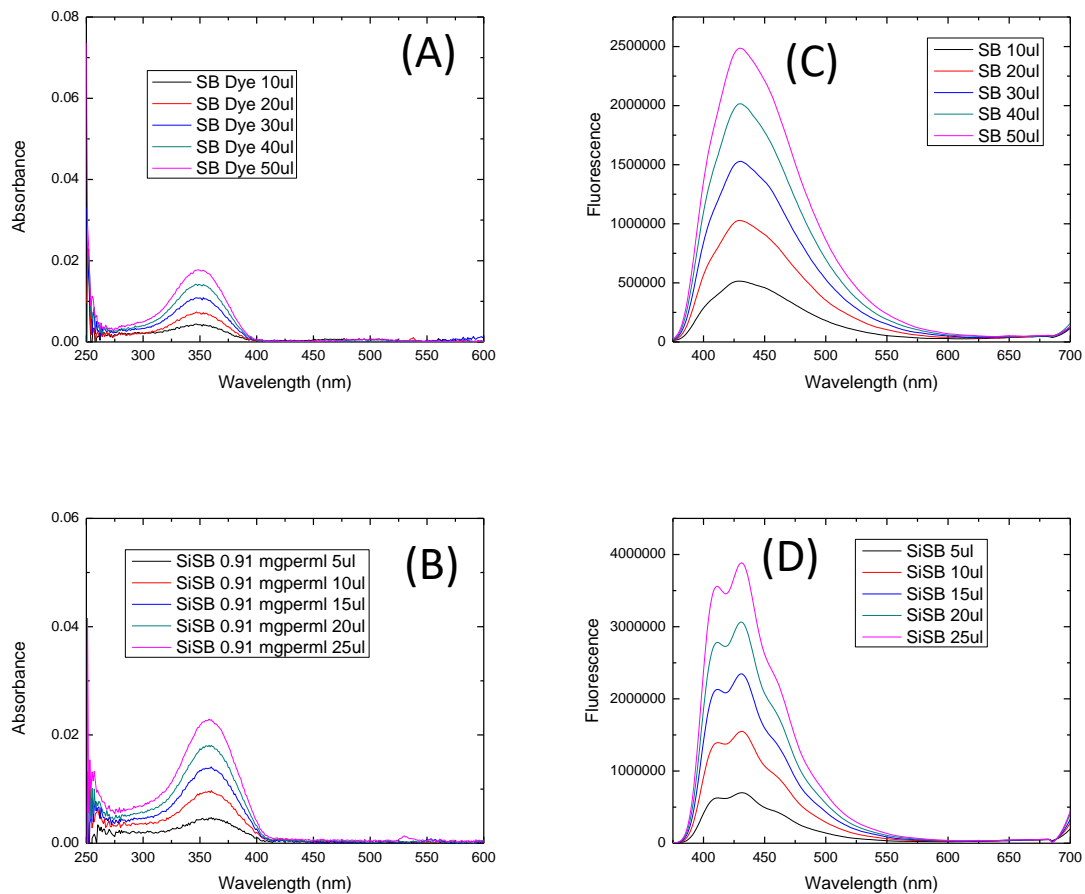


Figure S5: Absorbance (A and B) and fluorescence (C, and D) spectra of SB dye and SiSB particles respectively for quantum yield and brightness measurement.

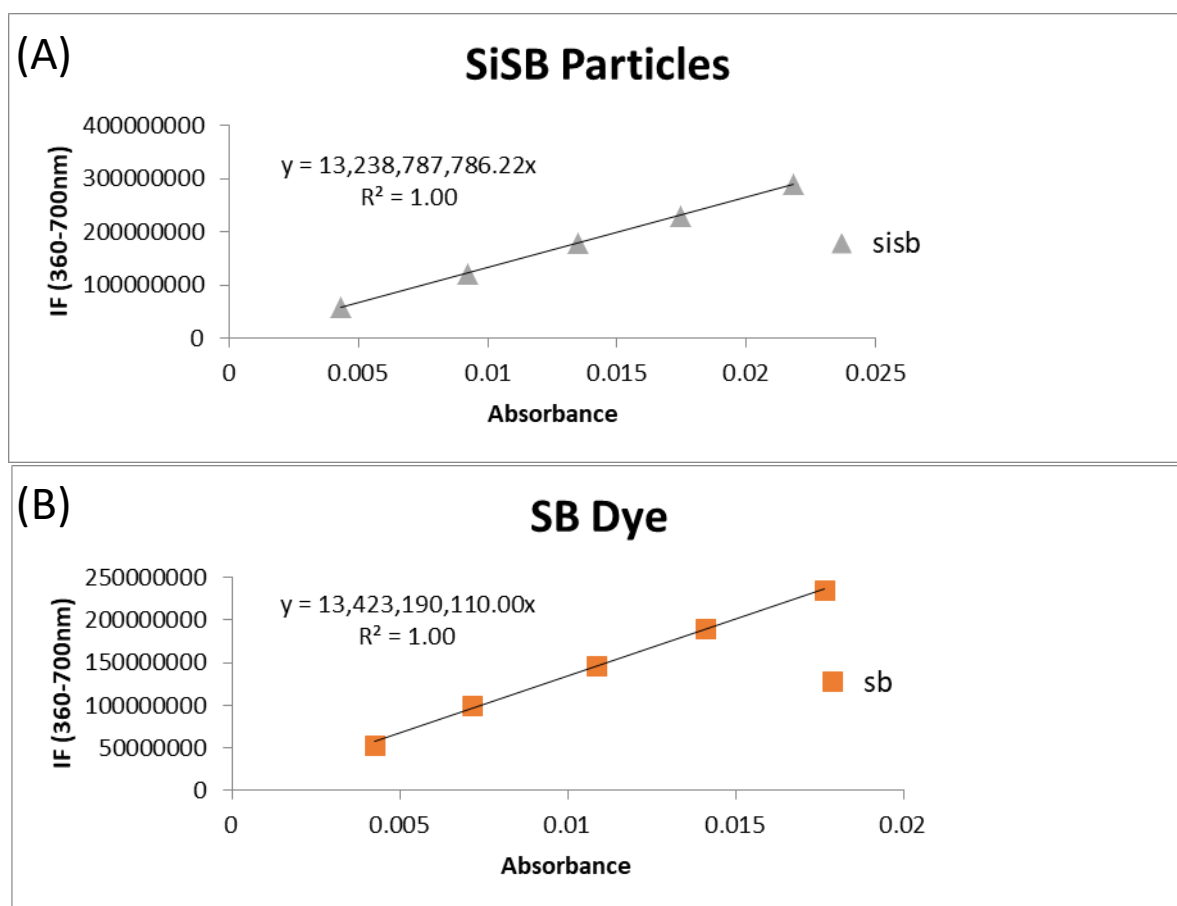


Figure S6: Concentration dependence of integral fluorescence (IF) of SiSB particles (A) and SB particles (B).

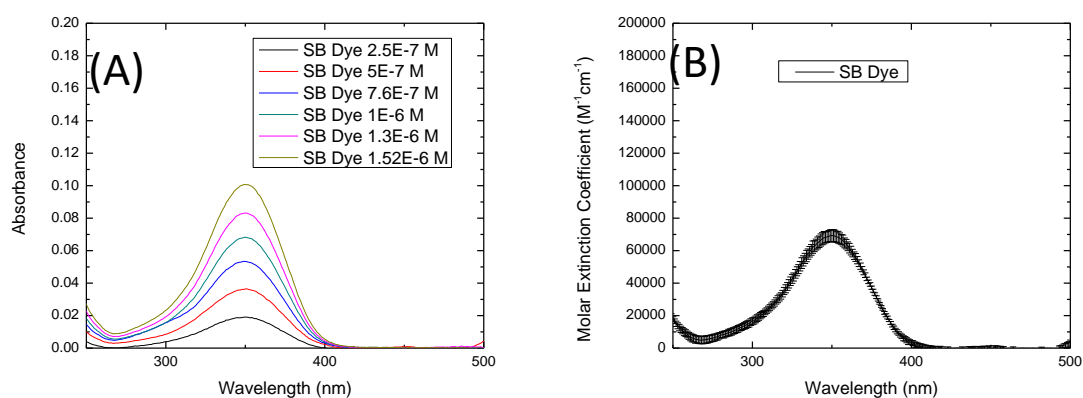


Figure S7: Absorbance (A) of stilbene 420 dye and the extinction coefficient (B) calculated using the absorbance and molar concentration of the dye.

QY of SB dye according to the literature⁵ is 0.82. The slope of IF vs. absorbance (figure S5) was used to determine the quantum yield of SiSB particles⁶. The QY of the sample –SiSB is given by,

$$\Phi_{SiSB} = \Phi_{SB\ Dye} \left(\frac{\text{Slope of IF vs absorbance of SiSB}}{\text{Slope of IF vs absorbance of SB Dye}} \right) \left(\frac{\eta_{SiSB}^2}{\eta_{SB\ Dye}^2} \right) \quad (S1)$$

where, Φ_{SiSB} is the quantum yield of the SiSB particles, $\Phi_{SB\ Dye}$ is the QY of SB dye (0.82), η_{SiSB} and $\eta_{SB\ Dye}$ are the refractive index of solvent (water) into which the SB dye and SiSB particles are added.

The brightness of particles relative to the dye (MESF units) as shown in table 1 is given by,

$$\text{Relative Brightness} = \frac{IF_{\text{particles @ } \lambda=360 \text{ to } 700\text{nm}} / \text{Number of particles}}{IF_{\text{Dye @ } \lambda=360 \text{ to } 700\text{nm}} / \text{Number of dye molecules}} \quad (S2)$$

Figure S5 shows a linear increase in fluorescence with increase in absorbance for both dye (S5A and S5C) and particles (S5B and S5D). These spectra were used for measuring quantum yield of the particles as shown in figure S6. The extinction coefficient of the dye was calculated using the absorbance and molar concentration of the dye as shown in figure S7. The number of dye molecules per particle and brightness were calculated using the spectra's showing in figure S8A and S8B respectively. Figure S9 shows that's SiSB-PEGFA particles are ~ 200 times brighter than SiFB-PEGFA particles while SiSB-PFFA particles are ~70 times brighter than SiFB-PFFA particles.

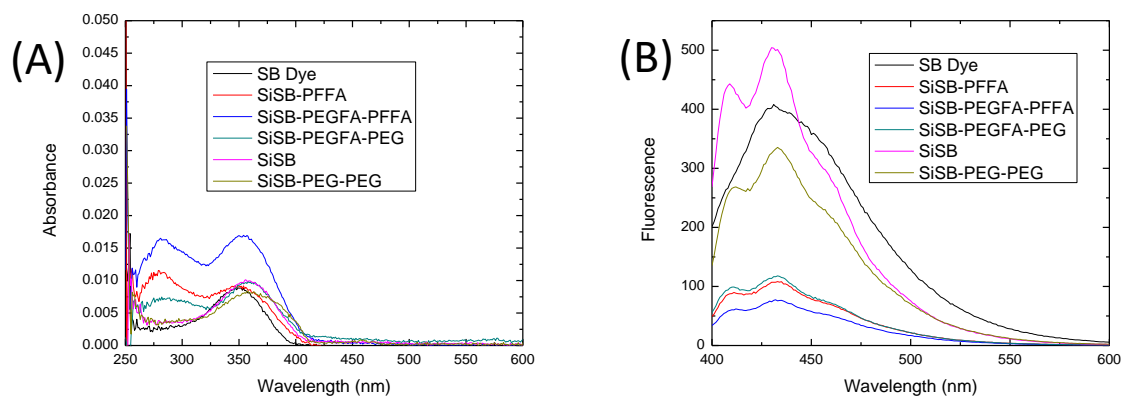


Figure S8: Absorbance (A) and fluorescence (B) spectra of particles used to estimate the number of dye molecules encapsulated and brightness relative to dye molecules respectively.

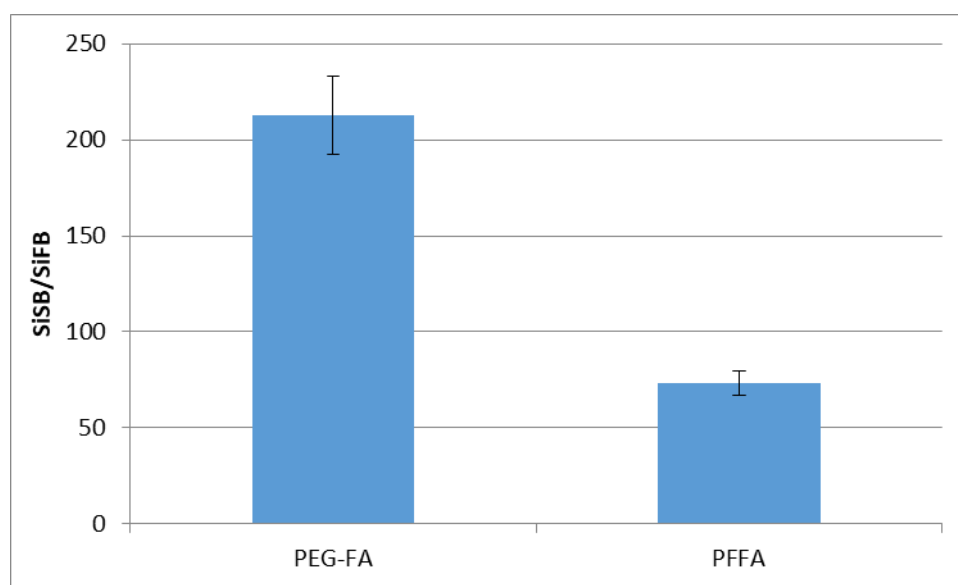


Figure S9: Ratios of the brightness of ultrabright (SiSB) nanoparticles and SiFB nanoparticles. Particles with PEG-FA and PFFA are shown. The brightness is an integral intensity in the range of 435-485 nm.

Table S5: Ratio of the brightness of different conjugation of particles with respect to SiSB-PEG particles.

Particles	Ratio of brightness
SiSB-PEGFA-PFFA:SiSB-PEG	0.10
SiSB-PEGFA:SiSB-PEG	0.22
SiSB-PFFA:SiSB-PEG	0.20
SiSB-PEG-PF127:SiSB-PEG	0.32
SiSB-PEG:SiSB-PEG	1.00
SiSB-PF127:SiSB-PEG	0.77

6. Tagging ability of UFMS particles using human cervical epithelial cancer (HeLa) cells in vitro

HeLa cells show over-expression of folic acid. To the best of our knowledge, the HeLa cell line used in this research is the same cell line as described in all existing publications ^{7, 8}. HeLa cells were grown at 70% confluency in DMEM medium supplemented with 10% Fetal Bovine Serum (FBS) at 37C and 5% CO₂. Nanoparticle stock solutions were pre-diluted directly into the growth medium, mixed and added to each well for a time course. After waiting for a predefined time, the particles were washed away with clear PBS buffer (rinsed twice) and were imaged in PBS buffer. Images are shown in Fig. S10 were acquired using EPI Fluorescent Inverted Microscope (TU2000 Nikon Co., Tokyo, Japan) or a Revolve Microscope (Echo, San Diego, USA). The images were taken using a 10x objective. The high-resolution imaging was done with the help of oil immersed 63x objective.

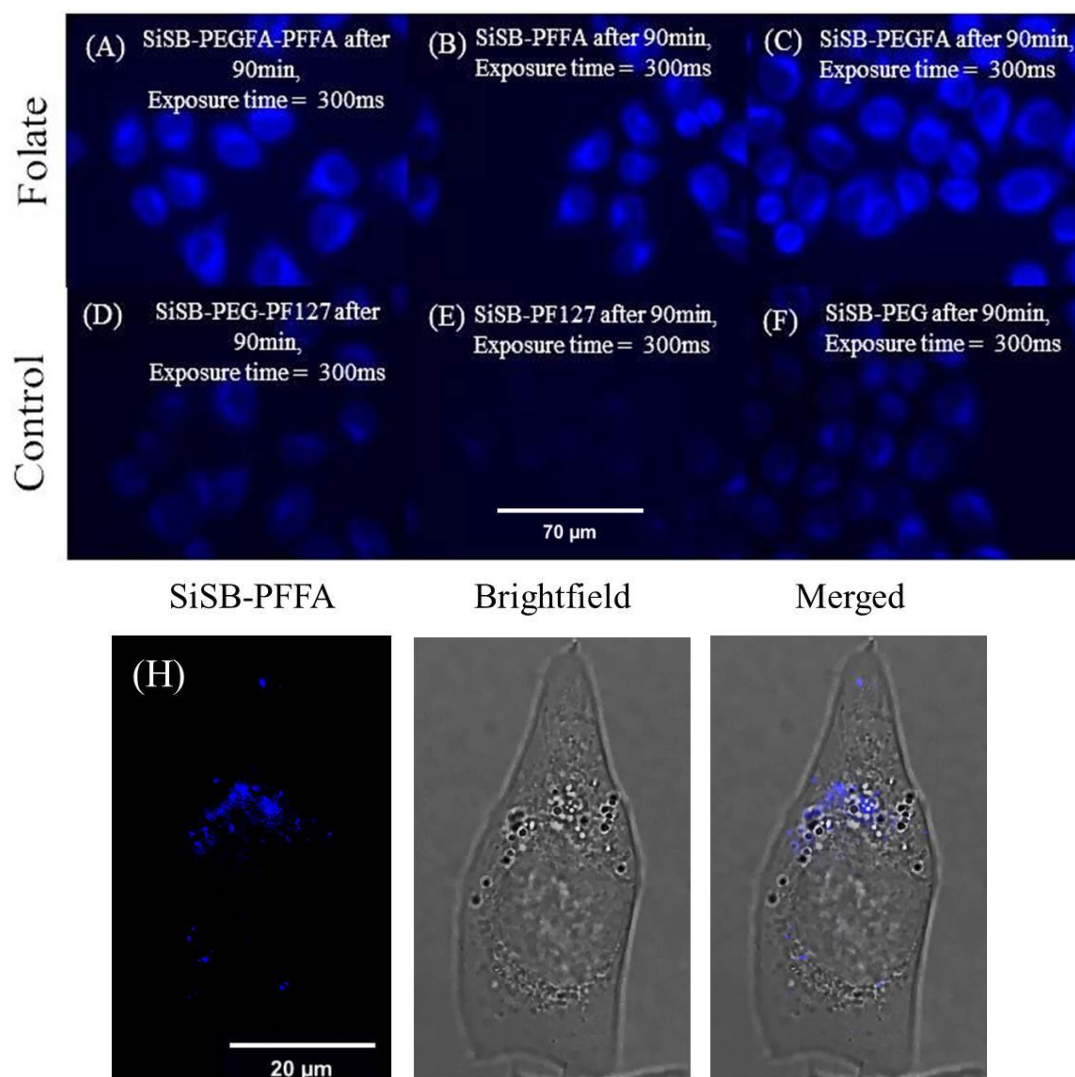


Figure S10: Testing of targeting ability of folate-functionalized particles in vitro.

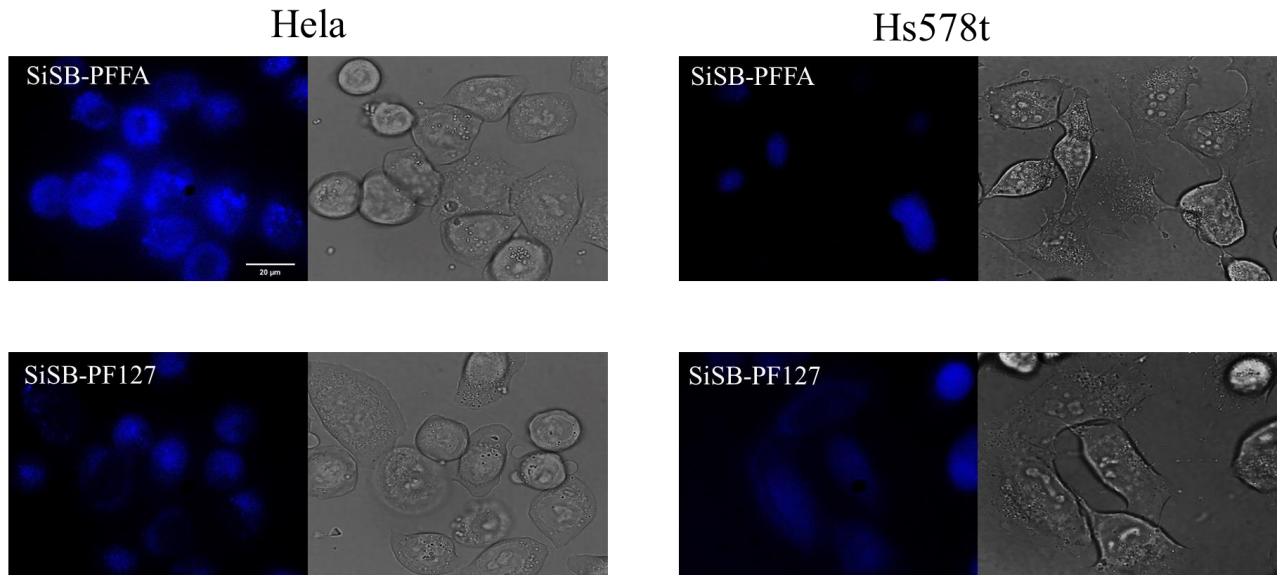
Comparing folate conjugated particles (A) SiSB-PEGFA-PFFA, (B) SiSB-PFFA and (C) SiSB-PEGFA and controls: (D) SiSB-PEG-PF127, (E) SiSB-PF127, and (F) SiSB-PEG. All particles were incubated with cells for 90 minutes. (H) An example of high-resolution targeting of HeLa cell with SiSB-PFFA particles.

It should be noted that the cells shown in figure S10 demonstrate a quite large number of particles are accumulated during 90 minutes of incubation. One cannot see individual fluorescent nanoparticles. A cell image in a high resolution and using a shorter time of incubation and a much lower concentration of nanoparticles is shown in Figure S10H.

7. Control experiments: Tagging ability of UFMS particles HeLa and Hs578t cells in vitro

Fig.S11 shows the preferential targeting of HeLa (overexpressed folate receptors) compared to Hs578t (low expression of folate receptors) cells using folate functionalized nanoparticles SiSB-PFFA and no folate control SiSB-PF.

(A)



(B)

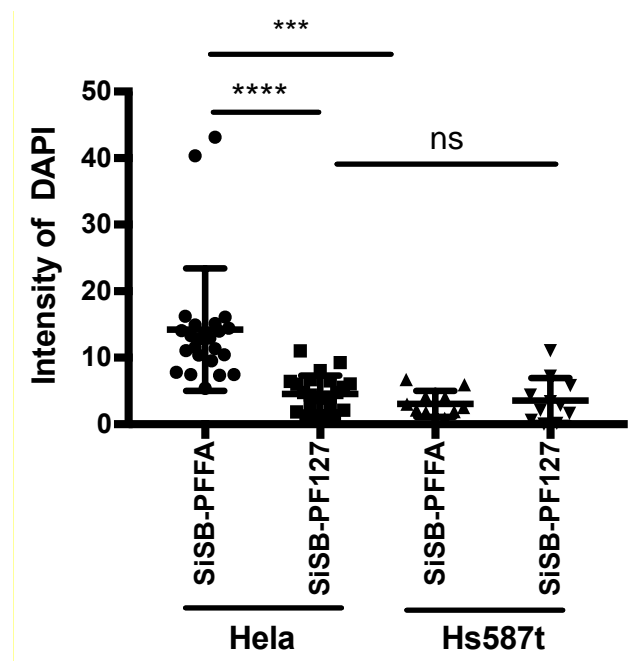


Figure S11: Comparison of targeting of Hs578t and HeLa cells using SiSB-PFFA and its control SiSB-PF UBFS nanoparticles. (A) The fluorescent (left) and brightfield (right) images of cells are shown. (B) Distributions of blue (DAPI) fluorescence intensity.

8. Tagging ability of UFMS particles using xenographic HeLa tumors in zebrafish in vivo

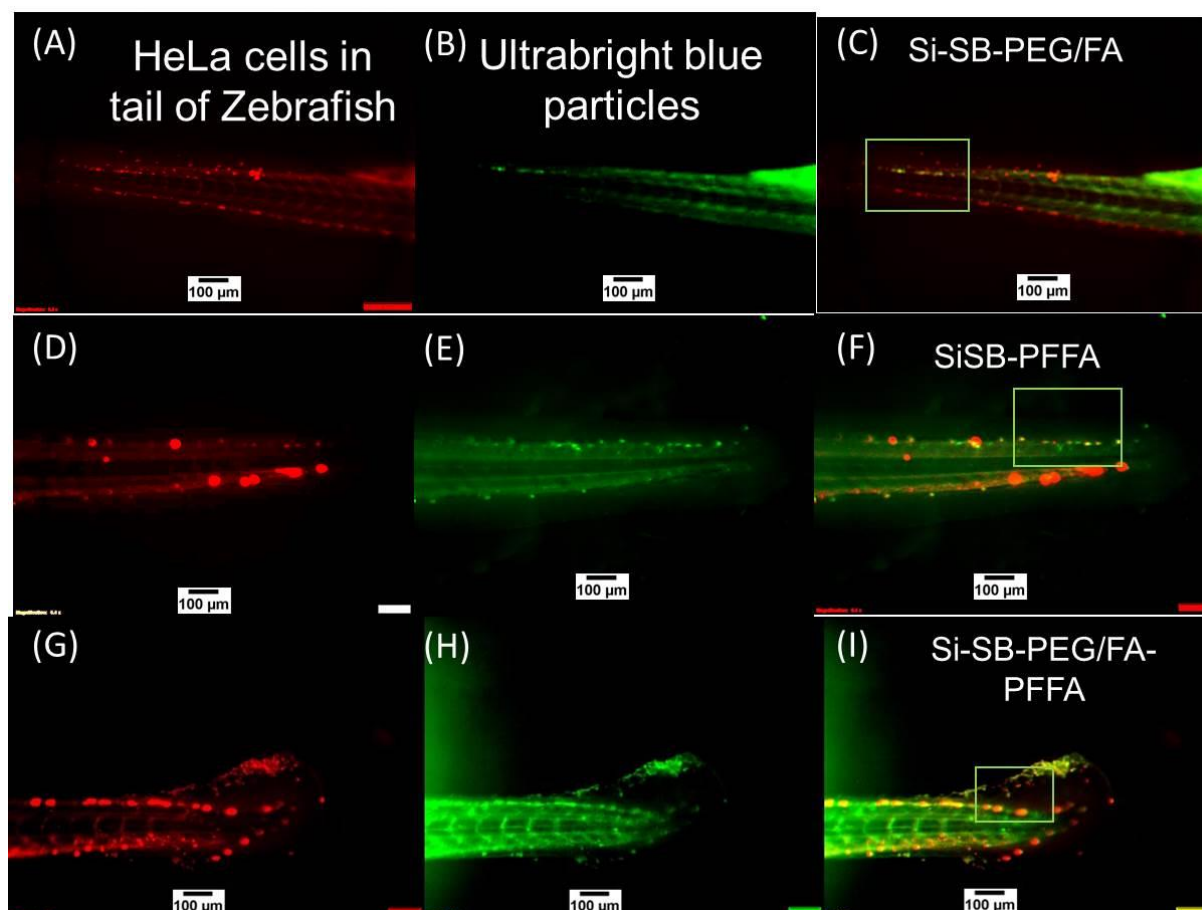


Figure S12: Co-localization of tumors and folate-functionalized UBFS nanoparticles. (Similar to Figure 3 of the main text but at lower magnification; zoomed areas shown in figure 3 are highlighted with green rectangles). Zebrafish injected with red fluorescent HeLa cells in the yolk (A, D and G). Ultrabright blue fluorescent particles functionalized with PEGFA-PEG (B), PFFA (E) and PEGFAPFFA (H) injected close to the eye of zebrafish. Corresponding colocalization images of red fluorescent cancerous cells and particles injected in zebrafish (C, F and I). Brightness and contrast of the particles images were optimized for better viewing while keeping the same values for all images. The images were taken after ~40 minutes past the particle injection.

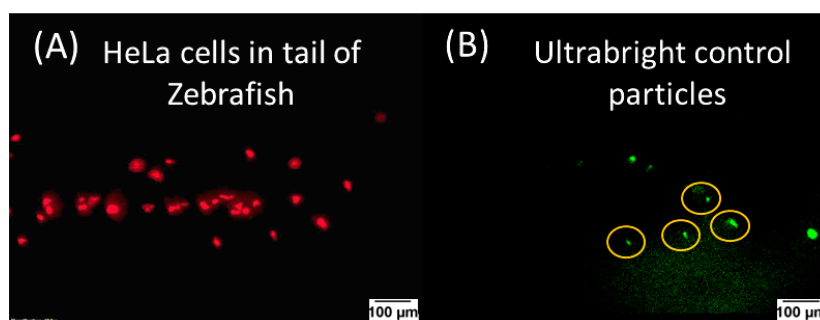


Figure S13: Zebrafish injected with red fluorescent tumors (HeLa cells) (A). Ultrabright blue (shown in green for better visualization) control SiSB-PF fluorescent particles functionalized (B). The images were taken after ~120 minutes past the particle injection.

9. Comparative targeting of HeLa and Hs578t cells

Figure S14 shows specificity of the targeting of SiSB-PFFA nanoparticles injected in zebrafish with xenograft HeLa and Hs578t cell tumors.

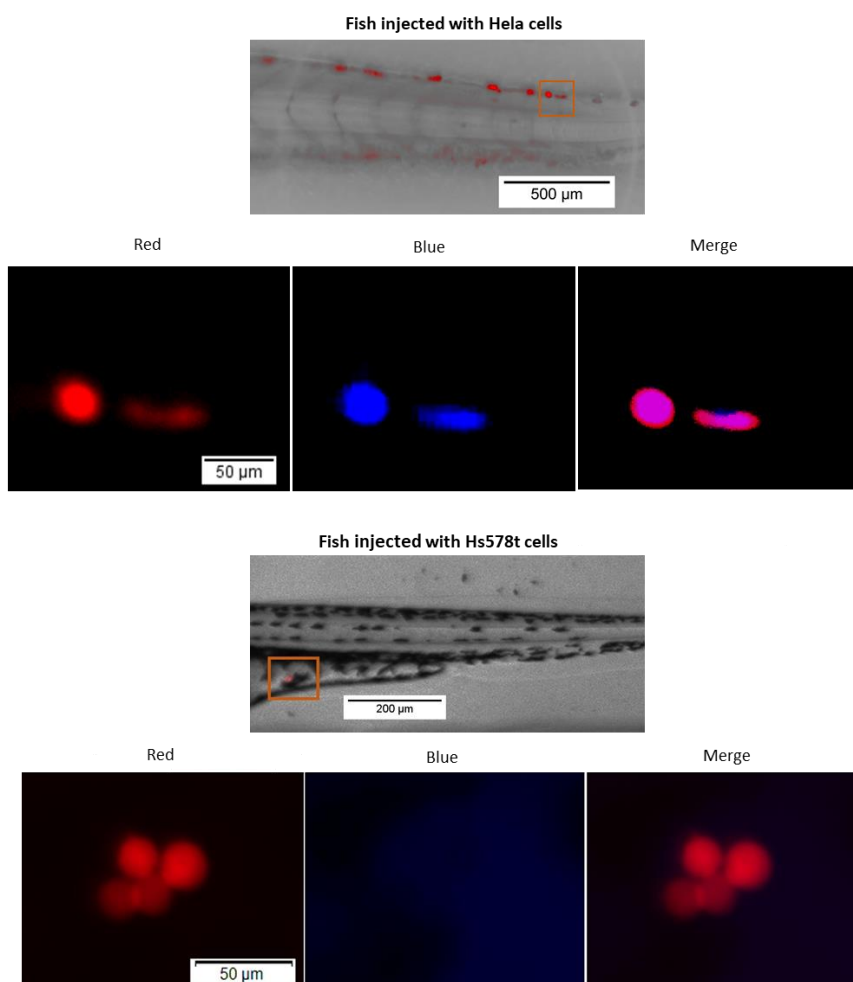
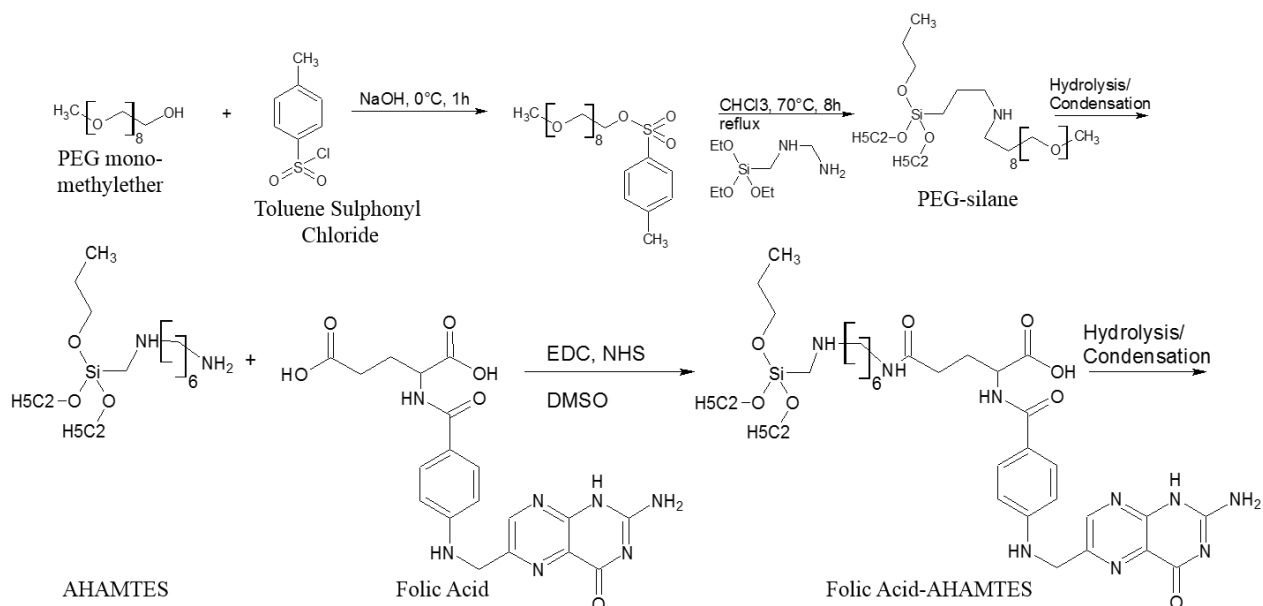
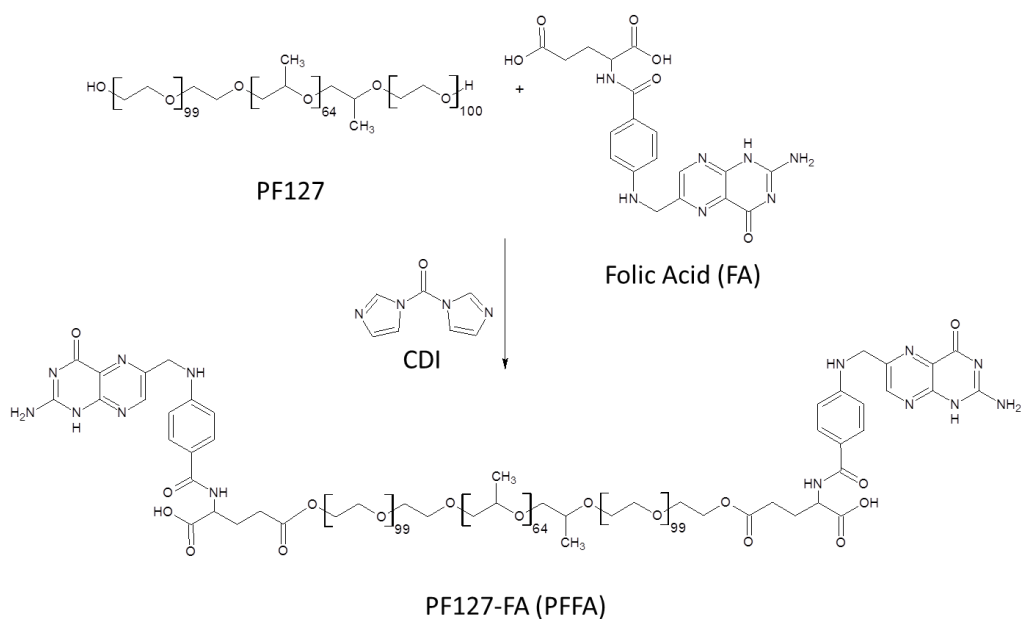


Figure S14: Comparative targeting of fish injected with HeLa and Hs578t cells.

10. Schematics of the synthesis



Scheme 1. Synthesis of PEG-Folate conjugates.



Scheme 2. Synthesis of PF127-Folate conjugates.

11. Zebrafish Image Processing: sensitivity calculation in zebrafish model

To do quantitative measurements with the obtained fluorescent images, the obtained images have to be corrected with respect to the fluorescent background, which may be slightly different in various images. To do that, a relative contrast is calculated as follows. To find the ratio of the tumor is to background and to correct the image background, intensity ratio $(I_t - I_{of}) / (I_b - I_{of})$ was used (this ratio is shown figure S15B). In this intensity ratio, I_t represents intensity from the tumor, I_{of} represents intensity outside of the fish and I_b represents background intensity from inside of the fish. For example, in figure S15A, the background intensity inside of fish I_b is 17 (arbitrary units), tumor intensity I_t is 44.5 and intensity outside of the fish I_{of} is 6.7. Hence, the intensity ratio for the tumor is to the background is ~ 3.7 . Figure S13 and S15 show the steps involved in image processing of zebrafish red cancerous cells and blue fluorescent UFMS nanoparticles to calculate relative contrast and sensitivity of detection of tumors with UFMS nanoparticles. Note that ratio $(I_t - I_{of}) / (I_b - I_{of})$ of 1.5 was taken as a threshold to define fluorescent targeting with UBFS nanoparticles. Yellow circles shown in figure S15B indicate the size of the potential location of tumors.

Figure S16 shows an example of the location of tumors (figure S16A) and UFMS particles (figure S16A). Blue fluorescence from particles was converted into green color for better visualization (figure S16B). Circles of multiple colors shown in this figure highlight locations used to calculate sensitivity and specificity: yellow circles show the co-locations of UFMS particles and tumors (true positive, TP), green circles indicate no-tumor places targeted by the particles (false positive, FP) and white circles indicate the areas in which there is neither tumors nor particles (true negative, TN). The areas not targeted by the particles but having tumor are false negative (FN). Sensitivity is defined as $TP / (TP + FN)$. In principle, we can estimate *specificity*, a parameter that is defined as the accuracy of defining the absence of cancer. It is equal to $TN / (TN + FP)$. It should be noted that the calculation of *specificity* is rather subjective because it is not well defined within this model. It simply means the absence of particles in the areas which are free of tumors. Obviously, the number of such organs can be quite large because particles simply cannot penetrate there, no matter if the particles are targeting (folate active) or control (no folate targeting).

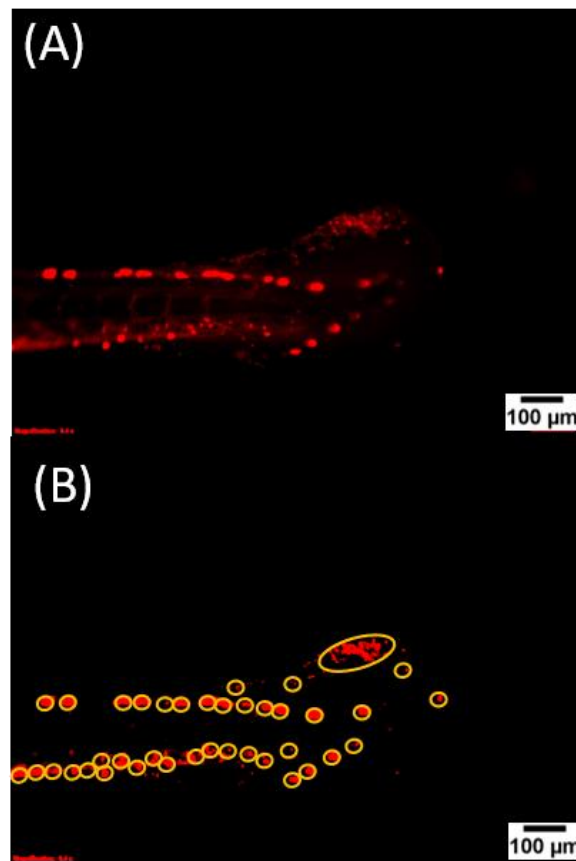


Figure S15: Image processing of zebrafish. Original images of zebrafish implanted with red tumors (A), and corresponding image after brightness and contrast correction (B). Note: The yellow circles indicate locations of the tumors.

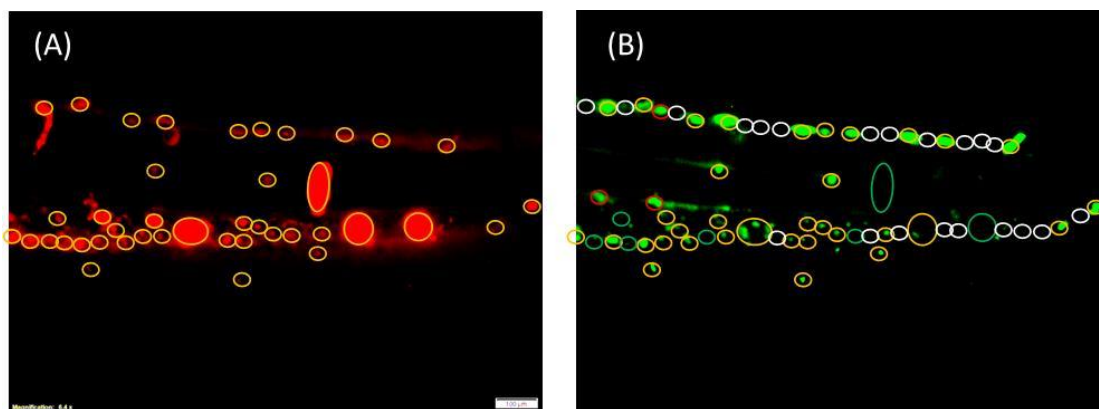


Figure S16: Image processing of zebrafish after injection of blue fluorescent nanoparticles. Original image of ultrabright blue fluorescent particles injected in zebrafish (A), $((I_t - I_{of}) / (I_b - I_{of}))$ ratio image (B). The blue color of particles was converted into green for better visualization. Yellow circles are shown in panel C highlight all locations used to calculate sensitivity and specificity. Circles of different color shown on panel B highlight specific locations used to calculate sensitivity and specificity: yellow circles show the locations of UFMS particles (true positive), green circles indicate non-specific highlighting by particles (false positive) while the white circles indicate areas of where there are neither tumors nor particles (true negative).

Sensitivity and specificity are estimated when using multiple folate-functionalized particles, Table S6. All the folate particles have high sensitivity and reasonably high (but lower) specificity. For example, SiSB-PFFA particles showed sensitivity and specificity of ~ 78% and 84% respectively for 3 different zebrafish. Although the sensitivity of SiSB-PFFA (78%) was slightly lower than SiSB-PEGFA (84%) particles, specificity seems to be higher than SiSB-PEGFA (75%) particles. This is consistent with the results from in vitro studies. The sensitivity of control non-folate particles SiSB-PF127 was much smaller than that of folate-functionalized particles, only ~15%.

Table S6: Sensitivity and specificity of different folate functionalized particles in zebrafish model demonstrated for different incubation times. The results for a control (SiSB-PEG) particles without folates are exemplified at the last row of the table.

		TP/(TP + FN)	TN/(TN + FP)
Particle type	time	Sensitivity (%)	Specificity (%)
SiSB-PEGFA	43 min	73	77
SiSB-PEGFA	80 min	94	74
SiSB-PFFA	76 min	81	77
SiSB-PFFA	255 min	83	87
SiSB-PEGFA-PFFA	56 min	86	71
SiSB-PEGFA-PFFA	60 min	81	75
SiSB-PF (control)	120 min	15	89

12. Cell toxicity study

12.1 Control Material

- Negative control for cytotoxicity: Serum free growth media (DMEM with 1% PSN, 1% Glutamax)
- Positive control for cytotoxicity: Triton X-100 (0.1%)

Test System: Transformed keratinocytes from histologically normal human skin (Addex Bio, Catalog T0020001, Lot #0000123)

Human keratinocytes (HaCaT) were grown in DMEM with 10% FBS, 1% PSN, 1% Glutamax for 2 days in 96-well plates to 95% confluence. Test samples were diluted in growth media (5-fold serial; 8 concentrations total; 6 replicates each) and incubated with cells (2×10^4 cells/well) overnight at 37°C. Cells were washed and a cell viability indicator was added (AlamarBlue; Invitrogen Cat# DAL1025). Cells were then incubated at 37°C for 4 hours and fluorescence (excitation: 540-570 nm; emission: 600 nm) was read on a 96-well plate reader.

The media-only blank was subtracted from the individual test sample values to remove non-specific assay effects. There was no appreciable effect of the samples on fluorescence at any concentration tested. Individual data outliers were identified and handled according to Q-test. Test sample fluorescence was normalized by dividing individual values by the negative control average (% of control). Normalized test sample fluorescence averages (\pm SD) were plotted as a function of the log of the test sample concentration (mg/mL). The CC₅₀ values were calculated for each test sample using a 4 Parameter Logistic (4PL) curve fit via GraphPad Prism.

12.2 Results

All four test samples demonstrated dose-dependent cytotoxicity. The effect of each test sample on HaCaT cell viability (fluorescence as a function of sample concentration) is shown in Figure S17. The CC₅₀ values calculated for each test sample as well as CPE data are shown in Table S7.

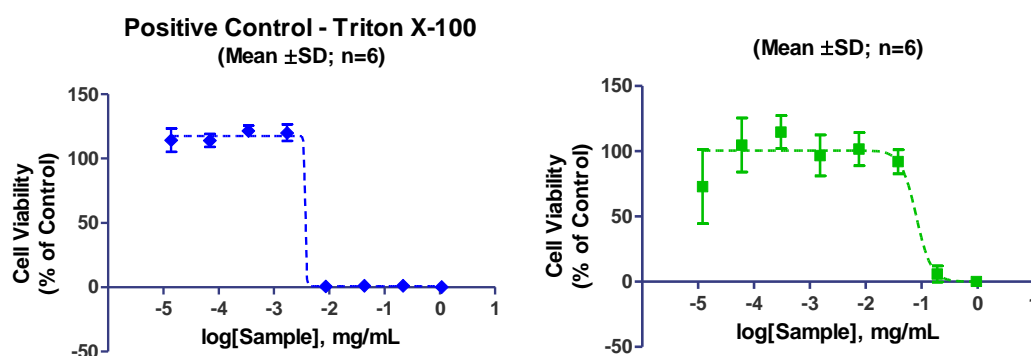


Figure S17. Cell viability plots. Positive control (left) and cell (right).

Table S7. Median Cytotoxicity (CC₅₀) Values

Test Sample	CC ₅₀ (mg/mL)	Lower CC ₅₀ (95% CI)	Upper CC ₅₀ (95% CI)
Mesoporous Silica NP	0.07963	0.05037	0.1259
Triton X-100	0.003697	0.00171*	0.00856*

*Confidence Interval (CI) was not calculated. The dilution just above and just below the calculated CC₅₀ value is provided.

13. Additional control experiments in vivo

Figure 17 shows the behavior of nanoparticles injected in zebrafish *without* HeLa cells.

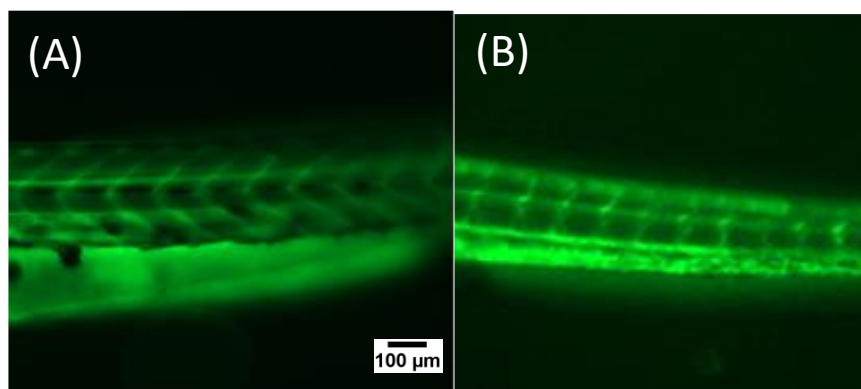


Figure S18: Control image of zebrafish with ultrabright blue nanoparticles (SiSB-PFFA) circulating in the vasculature after (A) 35 min and (B) 80 min after injection close to the eye of the zebrafish; red fluorescent HeLa cells were not introduced in the fish. The blue color of fluorescence was converted into green for better visualization.

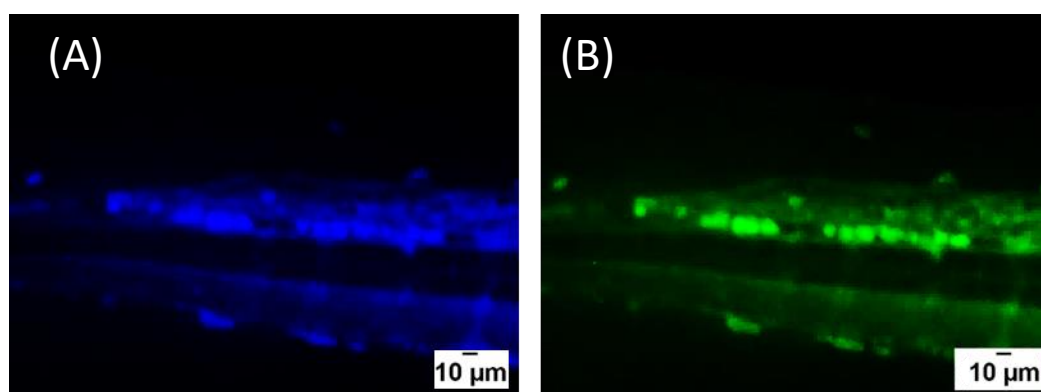


Figure S19: An example demonstrating the advantage of presenting blue (A) fluorescence in green (B). A better visualization for the human eye is clearly seen.

SUPPLEMENTARY REFERENCES

1. J. Chen, M. A. van Dongen, R. L. Merzel, C. A. Dougherty, B. G. Orr, A. K. Kanduluru, P. S. Low, E. N. G. Marsh and M. M. Banaszak Holl, *Biomacromolecules*, 2016, **17**, 922-927.
2. B. D. Smith, J. J. Higgin and R. T. Raines, *Bioorganic & medicinal chemistry letters*, 2011, **21**, 5029-5032.
3. I. V. Dimitrov, E. B. Petrova, R. G. Kozarova, M. D. Apostolova and C. B. Tsvetanov, *Soft Matter*, 2011, **7**, 8002-8004.
4. G. F. Ball, *Vitamins in foods: analysis, bioavailability, and stability*, CRC Press, 2005.
5. K. Smit and K. Ghiggino, *Dyes and pigments*, 1990, **13**, 45-53.
6. S. Palantavida, R. Tang, G. Sudlow, W. Akers, S. Achilefu and I. Sokolov, *Journal of Materials Chemistry B*, 2014, **2**, 3107-3114.
7. C. Leamon and P. Low, *Journal of drug targeting*, 1994, **2**, 101-112.
8. C. Leamon and P. Low, *Biochemical Journal*, 1993, **291**, 855-860.